

Article

Glassy Carbon Electrode Modified with C/Au Nanostructured Materials for Simultaneous Determination of Hydroquinone and Catechol in Water Matrices

Samuel Piña ^{1,2}, Christian Candia-Onfray ², Natalia Hassan ³, Paola Jara-Ulloa ⁴, David Contreras ¹ and Ricardo Salazar ^{2,*}

¹ Facultad de Ciencias Químicas, Universidad de Concepción (UDEC), Edmundo Larenas 129, Concepción 4070371, Chile; spina@udec.cl (S.P.); dcontrer@udec.cl (D.C.)

² Laboratorio de Electroquímica del Medio Ambiente, LEQMA, Facultad de Química y Biología, Universidad de Santiago de Chile (USACH), Casilla 40, Correo 33, Santiago 9160000, Chile; christian.candia@usach.cl

³ Programa Institucional de Fomento a la Investigación, Desarrollo e Innovación, Universidad Tecnológica Metropolitana (UTEM), Ignacio Valdivieso 2409, Santiago 8940577, Chile; nhassan@utem.cl

⁴ Facultad de Ingeniería y Ciencias, Universidad Adolfo Ibáñez, Diagonal Las Torres 2640, Santiago 7941169, Chile; paojara@gmail.com

* Correspondence: ricardo.salazar@usach.cl

Abstract: The simultaneous determination of hydroquinone and catechol was conducted in aqueous and real samples by means of differential pulse voltammetry (DPV) using a glassy carbon electrode modified with Gold Nanoparticles (AuNP) and functionalized multiwalled carbon nanotubes by drop coating. A good response was obtained in the simultaneous determination of both isomers through standard addition to samples prepared with analytical grade water and multivariate calibration by partial least squares (PLS) in winery wastewater fortified with HQ and CT from 4.0 to 150.00 μM . A sensitivity of 0.154 $\mu\text{A } \mu\text{M}^{-1}$ and 0.107 $\mu\text{A } \mu\text{M}^{-1}$, and detection limits of 4.3 and 3.9 μM were found for hydroquinone and catechol, respectively. We verified the reliability of the developed method by simultaneously screening analytes in spiked tap water and industrial wastewater, achieving recoveries over 80%. In addition, this paper demonstrates the applicability of chemometric tools for the simultaneous quantification of both isomers in real matrices, obtaining prediction errors of lower than 10% in fortified wastewater.

Keywords: simultaneous determination; modified electrode; nanomaterials; hydroquinone; catechol; chemometric tool



Citation: Piña, S.; Candia-Onfray, C.; Hassan, N.; Jara-Ulloa, P.; Contreras, D.; Salazar, R. Glassy Carbon Electrode Modified with C/Au Nanostructured Materials for Simultaneous Determination of Hydroquinone and Catechol in Water Matrices. *Chemosensors* **2021**, *9*, 88. <https://doi.org/10.3390/chemosensors9050088>

Academic Editor: Filippo Giubileo

Received: 22 March 2021

Accepted: 20 April 2021

Published: 24 April 2021

Publisher's Note: MDPI stays neutral with regard to jurisdictional claims in published maps and institutional affiliations.



Copyright: © 2021 by the authors. Licensee MDPI, Basel, Switzerland. This article is an open access article distributed under the terms and conditions of the Creative Commons Attribution (CC BY) license (<https://creativecommons.org/licenses/by/4.0/>).

1. Introduction

The determination of phenolic/polyphenolic compounds is a hot topic in the environmental, food and industrial fields [1]. Dihydroxybenzene compounds, such as hydroquinone (HQ) and catechol (CT), are toxic (100 μM in lymphocyte/human) and persistent in the environment [2–5]. For this reason, it is important to develop simple and fast analytical methods that allow the determination of HQ and CT, which generally coexist in wastewater because they have a similar molecular structure and chemical properties. The determination of HQ and CT is carried out by spectrophotometric or chromatographic methods after separation pretreatment processes, which requires long analysis times and large volumes of reagents. HQ and CT are electroactive compounds that can electrochemically oxidize on the surface of an electrode. The main difficulty in the simultaneous determination of both isomers lies mainly in the overlapping of the oxidation peaks, together with the loss of linearity in the voltammetric response due to competition between the two compounds for the electrode surface. Both problems can be solved by modifying the working electrode. In the last few years, many efforts have been devoted to developing modified electrodes able to increase the separation between both peaks together with the subsequent application of chemometric tools [6].

In recent years, a large number of analytical methods have been developed based on the use of nanomaterials. These methods have a wide variety of applications in bioanalysis, clinical analysis, pharmaceutical analysis, food safety and environmental analysis [7–10]. In particular, the use of nanomaterials for the modification of electrodes has generated great interest in environmental analytical chemistry. This is because, in general, these materials can significantly improve the conductivity and electrocatalytic activity of an electrical surface for a wide range of redox reactions, in addition to having a broad potential window and low electrochemical reactivity [11–13].

Carbon nanotubes (MWCNTs) are allotropes of carbon with a cylindrical nanostructure, in which a carbon-carbon link has a sp^2 - sp^2 hybridization. Usually, MWCNTs have a nanometric-scale diameter and a micrometer-scale length, which gives them attractive chemical, mechanical and electronic properties. In general, CTNs are divided into three groups: (1) Single-walled carbon nanotubes (SWCNT), (2) Double-walled carbon nanotubes (DWCNT) and (3) Multi-walled carbon nanotubes (MWCNT) [8–10]. SWCNTs have a cylindrical nanostructure formed by the winding of a graphite sheet in the form of a tube. In contrast, DWCNT and MWCNTs comprise several layers of concentrically ringed graphene, with a layer gap of 3.4 Å [14]. MWCNTs have been widely used to modify electrode surfaces due to their unique properties, such as high electrical and thermal conductivity, high chemical and mechanic stability, high area-volume ratio and high adsorption capacity. In addition, their properties increase the sensibility of electrochemical sensors to detect organic and inorganic compounds [15–21]. Moreover, the ease of immobilization and stability of proteins on MWCNTs have been widely used to manufacture electrochemical biosensors [22].

Furthermore, the use of metallic nanospheres has also become widespread in electroanalysis [23] due to their: (i) high effective superficial area, (ii) high mass transport, and (iii) catalytic activity [23,24]. Specifically, the study of gold nanospheres (AuNP) has been of interest because when they are deposited on the electrode surface, an increase in the charge transference and the superficial area is observed, and high sensibility and selectivity is achieved when analyses are performed [25]. One of the main ways of synthesizing AuNP is reducing a gold salt (generally HAuCl_4) in the presence of a stabilizing agent like citrate, through which the size and shape of AuNP can be controlled [26,27].

The modification of electrodes using different nanomaterials has resulted in an improved sensitivity for the determination of organic compounds in different matrices [11–13] and has led to electroanalytical methodologies with detection limits at μM and even nM concentration levels [28–30]. Several methods have been reported for the quantitative determination of organics in water, such as gas and liquid chromatography [31,32], UV-Vis spectrophotometry [33] and fluorescence [34]. In these methods, detection limits between 0.1 and 1.0 μM have been achieved, but they exhibit some disadvantages, such as complex pre-treatment of the sample and the use of high volumes of organic solvents. In this sense, electrochemical methods have sensitivities comparable with those of spectrophotometric and chromatographic methods, can be miniaturized to perform on-site determinations of contaminants of interest, require inexpensive equipment for their implementation and enable the quantification of several analytes simultaneously in a short time [12,35,36].

In the present work, we studied the simultaneous determination of HQ and CT in actual water samples using glassy carbon electrodes modified with three different multi-walled carbon nanotubes: (i) non-modified carbon nanotubes (MWCNT), (ii) carbon nanotubes modified with $-\text{COOH}$ (MWCNT-COOH) and (iii) carbon nanotubes modified with $-\text{NH}_2$ groups (MWCNT-NH₂) and decorated with gold nanospheres (AuNP). MWCNT-COOH and MWCNT-NH₂ produce better dispersion and increase the electrical conductivity of the modified electrode surface. The amino group of MWCNT-NH₂ can interact with different materials and has an excessive reactivity. Among these nanomaterials, AuNPs have been used as electrode materials due to their special properties in the electrocatalysis of organic and inorganic compounds.

2. Materials and Methods

2.1. Reagents and Materials

The HQ and CT employed were of analytical grade, provided by Sigma Aldrich and used as received. Analytical-grade water was used to prepare the solutions and dispersions. Boric acid EMPROVE[®], glacial acetic acid EMSURE[®] and orthophosphoric acid EMSURE[®] were provided by Merck.

Glassy carbon electrodes (GCE, model CHI104) were modified using different multi-walled carbon nanotubes separately: carbon nanotubes without functionalization (MWCNT) and functionalized with -COOH and -NH₂ groups (MWCNT-COOH and MWCNT-NH₂, respectively), all of them were provided by Dropsens. MWCNT dispersions were prepared in an Elma S 10 Elmasonic ultra-sonic bath with a concentration of 1.0 g L⁻¹ using water MilliQ as a dispersive agent. GCE was pre-cleaned by polishing using alumina powder of 0.3 and 0.05 μm consecutively and then washed with abundant Milli-Q water.

Gold nanoparticles (AuNP) were synthesized using citrate as stabilizing agent following the Turkevich methodology using HAuCl₄ as precursor [2], with a 20 nM of AuNP. AuNP (20 nM) and MWCNT/AuNP dispersions (1.0 g/mL of MWCNT on 20 nM AuNP dispersion) were prepared with Milli-Q water and then used to modify the GCE adding 10 μL on the electrode surface and then dried with nitrogen flux. AuNP were characterized by VIS-NIR spectroscopy using a Perkin Elmer Lambda 25 UV-VIS spectrometer, by Dynamic Light Scattering (DLS) using a NanoSizer-ZS Malvern Instrument and by Transmission Electronic Microscopy (TEM) with a Philips Tecnai 12 Biotwin microscope. The mixture of the MWCNT and AuNP was characterized by SEM in the LEO 1420VP instrument with a coupled Oxford 7424 dispersive energy analysis instrument at an acceleration voltage of 25 kV.

For the simultaneous determination of HQ and CT, solutions at different concentrations of both compounds were prepared in a 0.1 M buffer Britton–Robinson solution at pH 2.0.

2.2. Electrochemical Measurements

Cyclic voltammetry (CV) and differential pulse voltammetry (DPV) experiments were performed on a CH Instrument potentiostat CHI1140C. For the qualitative and quantitative electrochemical analysis, 10 mL of the solution was used in a traditional three-electrode electrochemical cell system. GCE with a geometric area of 0.126 cm² provided by CH Instruments was used as the working electrode, Ag/AgCl_{sat} as a reference electrode (CH Instruments) and platinum wire was used as counter electrode. In order to obtain the highest current response, different accumulation times were studied. Cyclic voltammograms were recorded between -1.0 and 1.0 V at a scan rate of 50 mV s⁻¹, under constant stirring at room temperature. The determination of HQ and CT performed based on their oxidation signal obtained by DPV with the following conditions: Step potential 4 mV, pulse amplitude 50 mV, pulse width 0.2 s, pulse period 0.5 s and deposition time of 30 s at 0.4 V as accumulation potential. The potential was scanned from 0.2 to 0.6 V. Electrodes do not need activation and washing step previous to the DPV analysis.

2.3. Simultaneous Determination of HQ and CT in Aqueous Matrices by Univariate and Multivariate Calibration

Four water samples of different types were obtained: (i) MilliQ water, (ii) drinking water, (iii) industrial wastewater from a winery industry, and (iv) river water. Subsequently, these samples were spiked with different concentrations of HQ and CT in the presence of 0.1 M Britton–Robinson buffer at pH 2.0. All the analyses were performed by DPV (10 mL of each solution) using the standard addition method and a multivariate calibration by Partial Least Squares (PLS). PLS was developed by Hermans and Svante Wold applying pattern recognition methods to instrumental data obtained from chemical systems. The algorithm is based on a bilinear model that uses Single Value Decomposition (SVD) in

matrix X that groups the voltammograms of each sample in relation to its concentration vector Y . Both matrices are decomposed into smaller matrices according to [37]:

$$X = TP^T + E \quad (1)$$

$$Y = UQ^T + F \quad (2)$$

where X and Y are the matrices of independent and dependent variables, respectively; T and U are the matrices of scores containing orthogonal rows to each other; P contains the loadings of matrix X ; E is the matrix of (residual) errors of matrix X ; Q corresponds to the loadings of matrix Y ; F is the error matrix of the vector Y . The B regression coefficients for the model are obtained according to:

$$B = W(P^TW)^{-1} \quad (3)$$

where matrix W contains the weights obtained by PLS, and it is constructed by relating the values of each value of the vector Y ($y_n = u$) according to:

$$w^T = \frac{u^TX}{u^Tu} \quad (4)$$

In PLS, the variables that show greater correlation with the response have extra weight because they are more efficient in prediction. In this way, linear combinations of the predictor variables are chosen that are highly correlated with the response variables and that are able to explain the variation of the response as a function of the predictor variables. The decomposition of matrix X is independent of matrix Y , where the direction of each latent variable of matrix X is modified until reaching the maximum covariance between this matrix and the concentration vector Y . This type of calibration has good results for the quantification of species in highly interfered matrices, provided that interferents are considered in the construction of calibration models [38].

3. Results and Discussion

3.1. Determination of HQ Using GCE Modified with Different MWCNTs

Cyclic voltammetry (CV) was used to characterize and studied towards HQ using the different MWCNTs in aqueous media. In order to obtain the highest current response, a previous pH study was performed in the range of 1.0–7.0 (Figure S1), indicating that the highest current for HQ oxidation is achieved at pH 2.0 for MWCNT-NH₂ and MWCNT-COOH systems. It has been reported that high faradaic currents are obtained for HQ oxidation in aqueous media and at low pH values when carbon-derived catalysts are used [39,40]. Furthermore, at more basic pH values, hydroxyl ions may interfere with the analysis due to the repulsion that they produce on dihydroxybenzenes with the electrode surface, preventing its oxidation and decreasing the faradic current [41]. Regarding these results, the following analyzes were performed at pH 2.0. Figure 1A shows the voltammograms recorded using the different materials in the absence of the HQ. An increase of the capacitive current was observed when a modified electrode was used. This increase was higher using the systems GCE/MWCNT-COOH and GCE/MWCNT-NH₂, followed by GCE/MWCNT. This change is related to the increase of the area of the modified electrodes and the better dispersion in water of the functionalized MWCNTs [42,43]. Furthermore, in Figure 1A, several faradaic processes between -0.5 to 0.5 V can be observed in the CV profiles of electrodes modified with carboxylate MWCNTs. These signals have been reported in the literature and are due to the presence of electroactive functional groups, such as ketones or aldehydes, which are generated in the functionalization process of carbon nanotubes [44]. The intensity of these signals may interfere in the analyte detection process, generating the distortion of the peaks obtained by CV or DPV, especially in the reduction step. Figure 1B shows the voltammograms recorded.

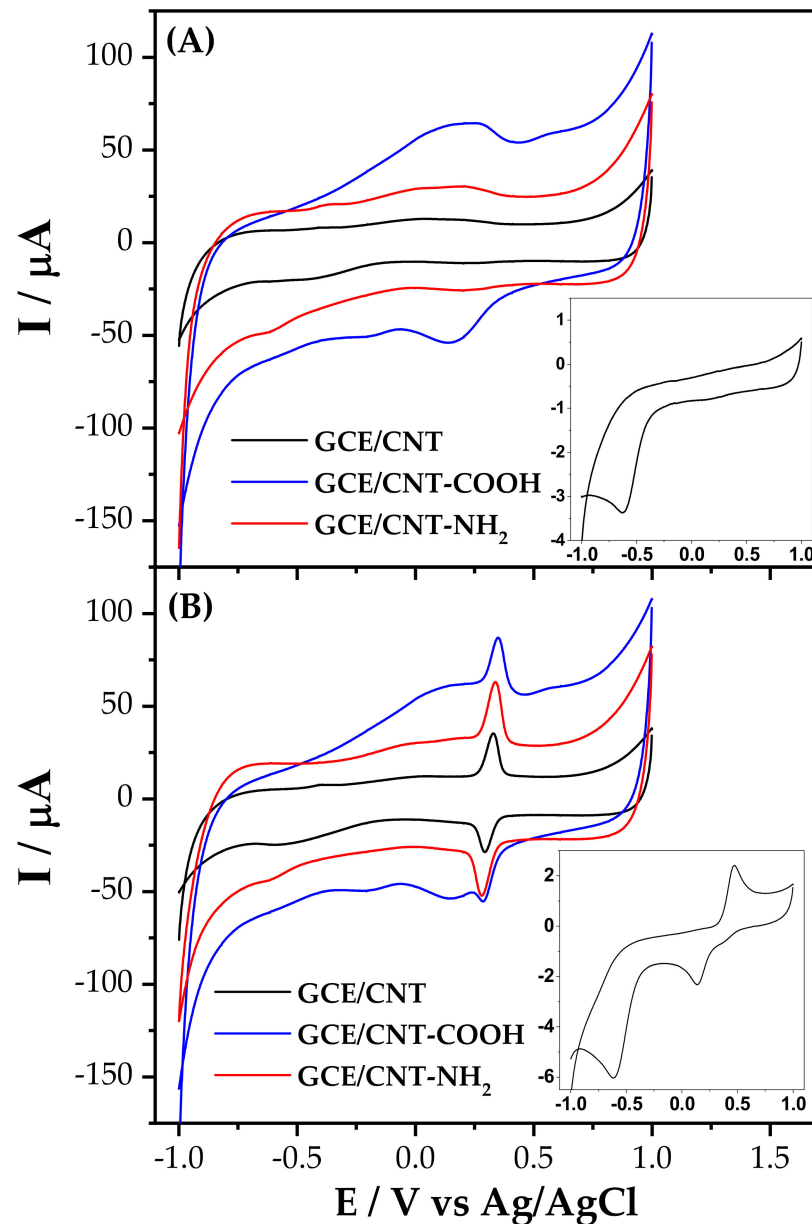


Figure 1. Cyclic voltammograms in the (A) absence and (B) presence of 0.1 mM of HQ using different electrodes (Inset: Cyclic Voltammogram of GCE-AuNP modified electrode). Experimental conditions: electrolyte buffer Britton–Robinson 0.1 M, pH 2.0, scan rate 50 mV s^{-1} , accumulation time 60 s.

In the presence of 0.1 mM HQ, oxidation and reduction peaks corresponding to the formation of quinone (Q) and HQ can be seen (Equation (5)) using all the electrodes; however, the intensity current for both oxidation and reduction peaks depends on the MWCNT used [45] (Figure 1B).



Additionally, the same figure shows a significant increase in the current peak for both oxidation and reduction peaks when MWCNTs are used; and this increase is higher when the MWCNTs are functionalized with -COOH and -NH₂ groups. An increase of 10.5 times and 13 times in the oxidation peak current compared to the GC electrode was observed using the GCE/MWCNT-COOH and GCE/MWCNT-NH₂ electrodes, respectively. However, there is a decrease in the resolution of the signals obtained with GCE/MWCNT-COOH,

which may be attributed to the presence of sp^3 carbon that forms the bond between the functional group and the MWCNT wall, thereby affecting the electron transfer [46,47]. The current and potential values for the redox process of HQ are summarized in Table S1.

Table S1 also shows the ΔE_p values. In the case of the electrode without modification, ΔE_p is 0.332 V, which indicates that the process is irreversible. By modifying the electrodes with MWCNTs, the redox process becomes reversible, obtaining smaller ΔE_p values close to the theoretical slope of Nernst (59.16 mV) [48]. There are considerable differences in the ΔE_p of the unmodified electrodes when compared to the electrodes modified with MWCNTs. First, a drastic decrease of the ΔE_p can be observed when using electrodes modified with MWCNTs; therefore, the redox process becomes more reversible when using nanotubes of carbon and shows an electrocatalytic effect on the reaction of HQ with the electrode surface. Second, a change in the mechanism is evidenced when using functionalized MWCNTs ($\Delta E_p \approx 59.16$ mV) instead of electrodes modified with non-functionalized carbon nanotubes ($\Delta E_p \approx 59.16/2$ mV). In this case, a transfer mechanism can be inferred via 2 electrons when using non-functionalized MWCNTs, and a mechanism via 1 electron when using functionalized nanotubes. This could be attributed to the adsorption of HQ due to the functional groups present on the surface of MWCNTs, which promote the transfer kinetics of one electron. Third, the currents obtained using electrodes modified with functionalized MWCNTs are higher than the currents obtained using electrodes modified with MWCNTs. Following the previous idea, the change of mechanism could explain the difference in current between the functionalized and non-functionalized material since the multiple transfers of electrons usually involves chemical stages that generate intermediaries in the reaction that could undermine the electronic transfer process, reducing the current peak obtained and resulting in a loss of sensitivity [49].

Since the GCE/MWCNT-COOH and GCE/MWCNT-NH₂ systems present a higher current response, the following analyses were performed using only these systems.

3.2. Accumulation Time Effect on the Oxidation of HQ

The effect of accumulation time on the current intensity was studied for the systems GCE/MWCNT-COOH and GCE/MWCNT-NH₂ (Figure 2). For both systems, an increase of the current was achieved with the accumulation time until reaching a maximum value, and then the current decays. The maximum current was achieved at 180 s and 30 s for GCE/MWCNT-COOH and GCE/MWCNT-NH₂, respectively. During the accumulation time, large amounts of HQ molecules are rapidly adsorbed to the surface of the carbon nanotubes due to strong electrostatic forces at the start of the adsorption process. The decrease in current obtained after the optimal accumulation time can be explained due to the gradual occupation of the MWCNT surface by the HQ molecules, where competitive adsorption is inevitable. The HQ molecules that are not absorbed diffuse from the outer Helmholtz plane towards the bulk of the solution, increasing the adsorption resistance and decreasing the adsorption rate of HQ. Furthermore, it can be seen that under the same conditions, MWCNT-NH₂ presents a higher adsorption capacity, indicating that the conditions are favorable for HQ adsorption. This property would improve the migration of the analyte to the electrode surface, in addition, to provide a larger surface for the accumulation and formation of double electrical layers, resulting in more sensitive electrochemical signals for the detection of these species in aqueous matrices. Accordingly, the following studies were performed using an accumulation time of 180 s and 30 s for the systems GCE/MWCNT-COOH and GCE/MWCNT-NH₂, respectively. Similar results were observed for the oxidation of CT under the same experimental conditions.

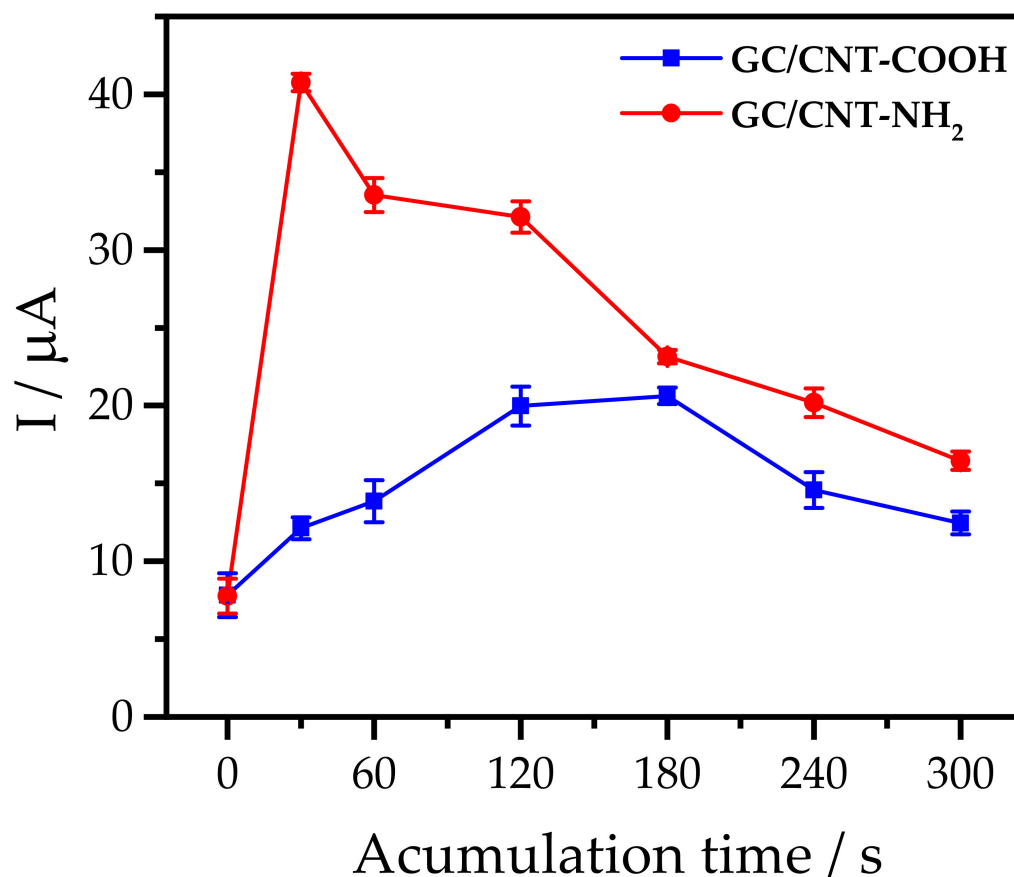


Figure 2. Effect of accumulation time on the oxidation current intensity of 0.1 mM HQ for the GCE/MWCNT-COOH and GCE/MWCNT-NH₂ systems. Working conditions: Scan speed 50 mV/s, Electrolyte: Buffer Britton–Robinson 0.1 M, pH 2.0.

3.3. Determination of HQ Using GCE Modified with Different MWCNTs and AuNP

Before using AuNPs in the electrochemical system, they were characterized by TEM, UV-Vis-NIR spectroscopy and Dynamic Light Scattering. TEM analyses (Figure 3A) showed that AuNP presents a homogeneous and quasi-spherical shape, and their size is between 12–13 nm with an average size of 12.7 ± 2 nm. The size was confirmed by UV-VIS-NIR (inset Figure 3A) analysis, which shown a maximum of the band at 518 nm. This value corresponds to symmetric surface plasmon absorption and quasi-spherical particle of 12–18 nm [26,50]. DLS analyses (Figure S2) agree with the AuNP size with a 12.7 ± 2 nm value. The MWCNT-NH₂ and AuNP mixture was characterized using SEM (Figure 3B), and images showed that AuNP was dispersed homogeneously on the MWCNT-NH₂ surface, which indicates a good interaction between the nanospheres and the amino groups present in the nanotubes, enabling the electrostatic deposition of the AuNP on the rough surface of the functionalized MWCNTs.

The effect of the AuNP towards the HQ detection using MWCNT-COOH and MWCNT-NH₂ was studied using cyclic voltammetry (Figure 4A,B, respectively). An increase of faradaic current was observed using AuNP and the different MWCNTs; however, more reversible and defined current peaks were obtained for the HQ/Q couple using GCE/MWCNT-NH₂-AuNP. As seen in Figure 3B, good interaction between AuNP and MWCNTs was assessed, which would create a synergistic effect on the HQ detection, thereby generating an increase in the current due to a better electronic transfer attributed to the contribution of both materials. The different peak potentials and currents for the HQ oxidation using both systems are summarized in Table S2. A poor signal was observed using only GCE/AuNP (Inset Figure 4B), which could be attributed to (i) the incapacity

of GCE's surface to adsorb AuNP due to the lack of functional groups that promote the electrostatic interaction between the nanoparticles and the surface of the electrode, and (ii) AuNP present a smaller surface area compared to the electrodes modified with MWCNTs.

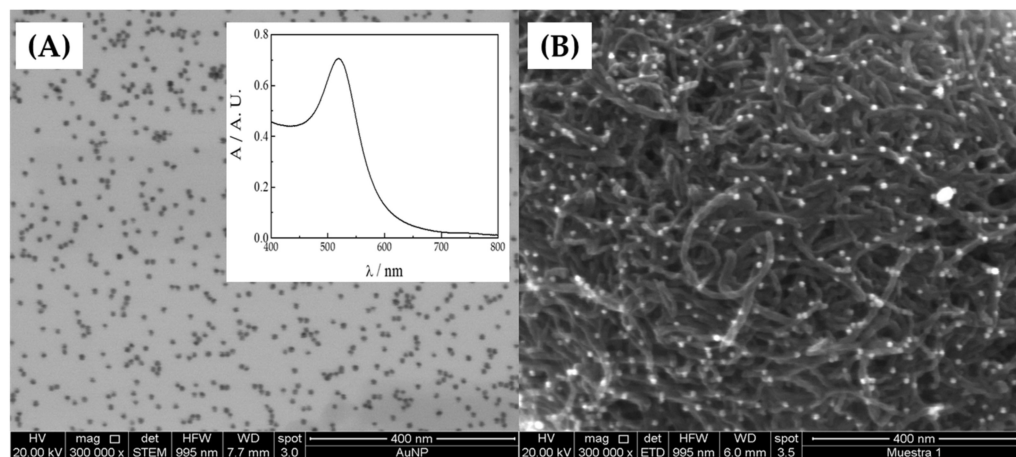


Figure 3. (A) Transmission Electron Microscopy (TEM) and AuNP characterization, (Inset) VIS-NIR spectroscopy made for AuNP solution. Experimental conditions: Zeta potential: -20.3 mV. (B) Scanning Electron Microscopy (SEM) made to GCE/MWCNT-NH₂-AuNP.

Since the highest current was obtained using GCE/MWCNT-NH₂-AuNP, the following experiments were performed using only this system.

3.4. Simultaneous Determination of HQ and CT Using MWCNT/NH₂-AuNP

In order to clarify the transport mechanism of HQ towards the surface of the modified electrode, the effect of the variation of the scanning speed on the performance of MWCNT-NH₂/AuNP was studied. With the increase of the sweep speed from 5 to 200 mV s⁻¹, the peak currents for HQ and CT increased continuously, where I_{pa} and I_{pc} showed a linear and proportional response to the square root of the scan rate ($v^{1/2}$), obtaining a slope of 0.48 for HQ and 0.49 for CT. Since both slopes are close to 0.5, the electrooxidation process of HQ and CT is controlled by diffusion, according to the Randles–Sevcik equation.

To assess the interference in the simultaneous determination of HQ and CT, we proceeded to study the oxidation of both analytes by DPV, considering that HQ and CT have an oxidation peak separated by 100 mV when analyzing each analyte alone using DPV. Figure 5A shows the voltammograms of different HQ concentrations with a constant concentration of CT 50 μ M. The peak current is increased linearly when increasing the concentration of HQ in a range of 4.25–150.00 μ M with $R^2 = 0.9995$ and a $F_{exp} = 0.0004$ (Critical F _[0.05,72,52] = 1.53) with a linear equation of I_p (μ A) = $-12.796 + 1.539$ [HQ] (μ M). The same procedure was followed for the CT calibration curve, keeping a constant HQ concentration of 50.0 μ M.

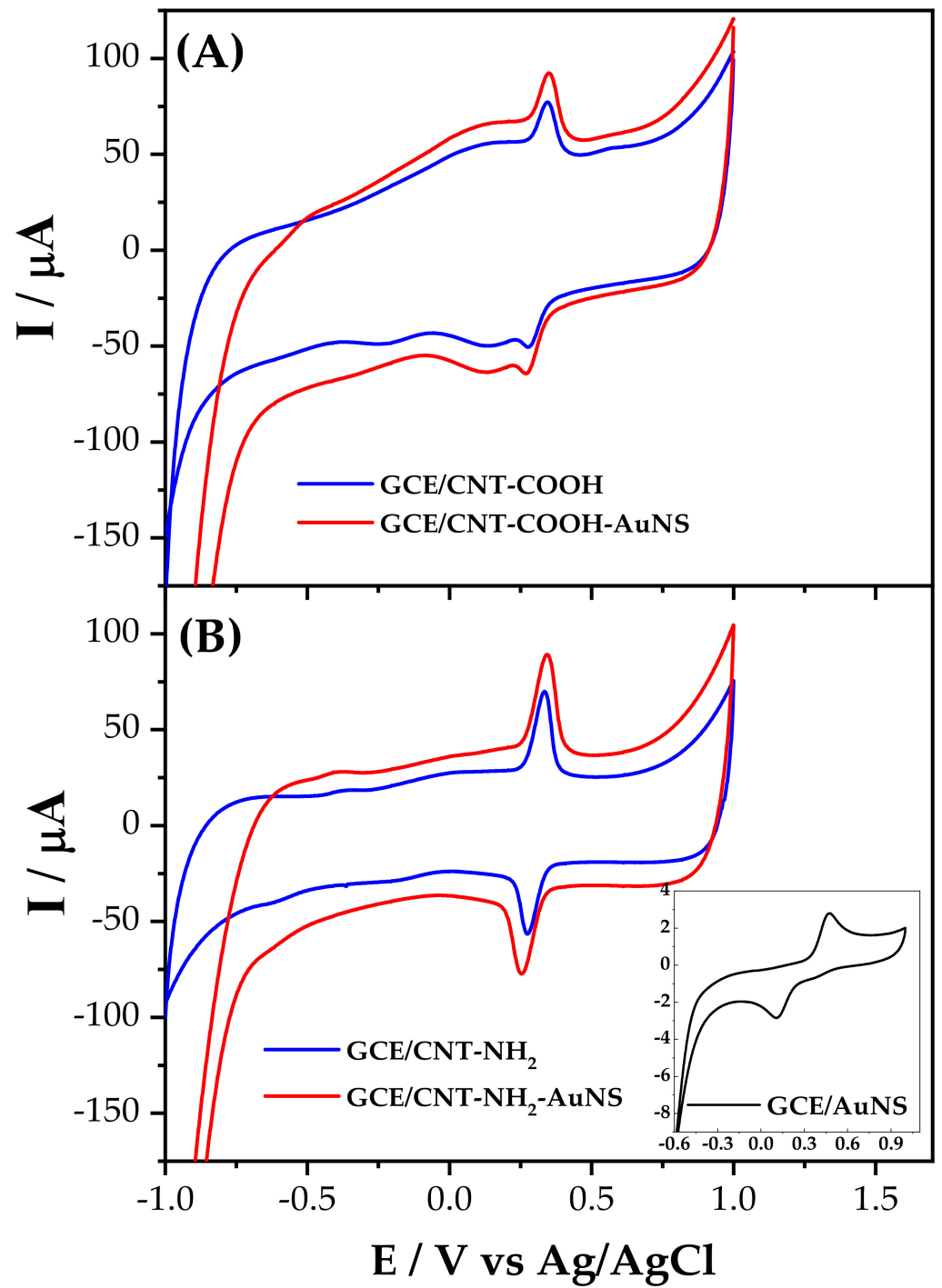


Figure 4. Cyclic voltammograms in the presence of 0.1 mM HQ using the different systems of MWCNT and AuNP. (A) MWCNT-COOH (Inset: Cyclic Voltammogram of AuNP modified GCE) with an accumulation time of 180 s, (B) MWCNT-NH₂ with an accumulation time of 30 s. Experimental conditions: electrolyte buffer Britton–Robinson 0.1 M, pH 2.0 and scan rate 50 mV s⁻¹.

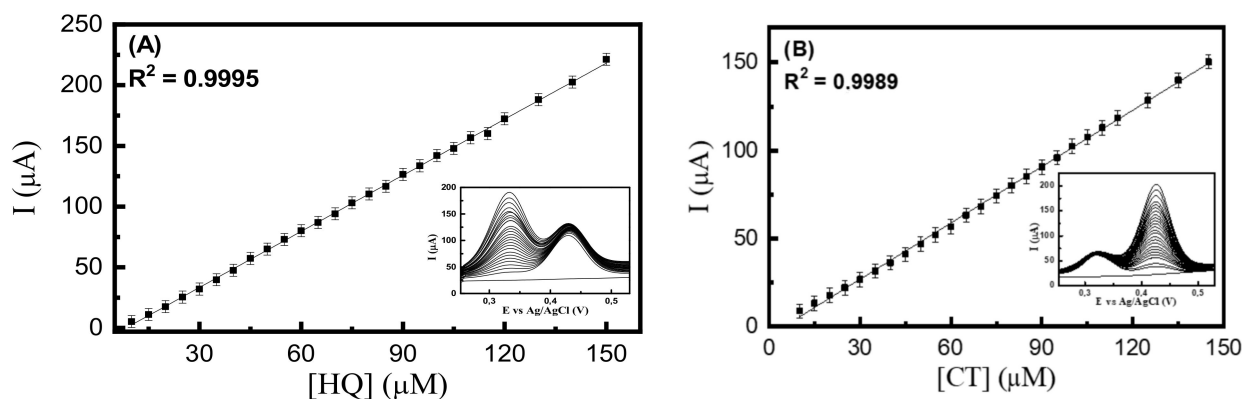


Figure 5. Oxidation voltammograms and calibration curve of (A) HQ in the presence of 50.0 μM CT and (B) CT in the presence of 50 μM of HQ. Working conditions: Medium Britton–Robinson pH 2.0 Swept speed: 0.004 V s^{-1} , Accumulation time: 30 s.

In the differential pulse voltammograms in Figure 5B, the peak current is observed to increase as the concentration of CT rises. In addition, the signal corresponding to HQ does not significantly affect the current intensity or the oxidation potential value in the measurements, having a separation peak of $>100 \text{ mV}$, approximately. The calibration curve for CT shows a good linear relationship in the presence of HQ, with a linear range between $3.91\text{--}150.00 \mu\text{M}$ and $R^2 = 0.998$ and a $F_{\text{exp}} = 0.0026$ (Critical $F_{[0.05,72,52]} = 1.53$) according to equation $I_p (\mu\text{A}) = -5.142 + 1.067 [\text{CT}] (\mu\text{M})$. In oxidation, the voltammograms of HQ and CT show a peak separation of 120 mV , which allows the differentiation of the compounds using the MWCNT-NH₂-AuNP electrode. A decrease in sensitivity during simultaneous determination can be observed when comparing the calibration curve of separated species. For HQ, the sensitivity in simultaneous determination is $1.549 \mu\text{A } \mu\text{M}^{-1}$, and determination has an initial value (in the absence of CT) of $6.857 \mu\text{A } \mu\text{M}^{-1}$ (corresponding to a decrease of 77.4%). In the CT case, sensitivity decreases in the simultaneous determination of the analyte in the presence of HQ. Initially, without HQ, sensitivity was $6.779 \mu\text{A } \mu\text{M}^{-1}$; however, when the solution contained $50 \mu\text{M}$ of HQ, a sensitivity of $1.067 \mu\text{A } \mu\text{M}^{-1}$ was achieved for CT, decreasing to 84.3%. Although peak potentials diverge above 100 mV , an overlap is seen between the signals when the HQ faradaic process ends and the CT oxidation process begins (between 0.400 and 0.420 V), which could decrease the sensitivity in the simultaneous determination of both isomers. The great decrease in CT sensitivity in the presence of HQ could be because HQ oxidizes at lower potentials than CT. This redox process would interfere at the beginning of the oxidation of catechol. The experimental analytical parameters of the method were determined, and the results obtained from the validation are presented in Table 1. The limit of detection (LD), the limit of quantification (LQ) and linearity parameters were calculated using the modern definition of IUPAC [51], which considers type α and β errors based on the residual error of the calibration curve and the instrumental error (pure error) with an $\text{LD} \approx 1.0 \mu\text{M}$ and $\text{LQ} \approx 4.0 \mu\text{M}$ for both analytes. The limits calculated according to the old IUPAC definition [52] are $\text{LD} = 0.98$ and $\text{LQ} = 4.12$ for HQ and $\text{LD} = 0.77$ and $\text{LQ} = 3.59$ for CT. The limits reported in Table 1 correspond to the current definition of LD and LQ according to IUPAC, since the old definition provides over-optimistic values that could lead to α -errors and β -errors (false positive and false negative, respectively). The linear range selected for the determination of analytes ranges between $4.00\text{--}150.00 \mu\text{M}$. We studied the accuracy of the MWCNT-NH₂-AuNP electrode in $n = 15$ determinations, obtaining a coefficient of variation of 2.2% for HQ and 2.1% for CT, which showed similar precision in a succession of repeated measurements for both analytes.

Table 1. Comparison of different sensors reported for the simultaneous determination of HQ and CT.

Material	Analyte	Sensitivity	Lineal Range/ μM	LD/ μM	LQ/ μM	ΔE_p (HQ-CC)/mV	Technique	pH	Ref																																																																																																				
Graphene screen-printed electrodes	HQ	1.3221 μM	n.d.	2.7	9.1	105	DPV	7.0	[6]																																																																																																				
	CC	1.5825 μM	n.d.	1.7	5.6					NDSBAC ¹	HQ	0.9997 μM	0.5–300	0.11	n.d.	112	DPV	6.5	[53]	CC	1.0662 μM	0.5–300	0.09	n.d.	WBC/Au-850-15 ²	HQ	164.4 $\mu\text{A } \mu\text{M}^{-1} \text{ cm}^{-2}$	0.008–1	0.002	n.d.	112.8	DPV	6.0	[54]	CC	132.0 $\mu\text{A } \mu\text{M}^{-1} \text{ cm}^{-2}$	0.01–1.0	0.004	n.d.	AuNPs-MPS ³	HQ	n.d.	10.0–1000.0	1.2	n.d.	123	SWV	7.0	[55]	CC	n.d.	30.0–1000.0	1.1	n.d.	GR-GO	HQ	n.d.	0.5–300	0.16	n.d.	102	DPV	7.0	[56]	CC	n.d.	0.5–300	0.2	n.d.	NiO/MWCNT	HQ	n.d.	10–500	2.5	n.d.	~110	DPV	7.0	[57]	CC	n.d.	10–400	2.5	n.d.	GO-TT-MWCNT	HQ	n.d.	0.01–200	0.035	n.d.	n.d.	DPV	7.4	[58]	CC	n.d.	0.5–200	0.049	n.d.	MWCNT-NH ₂ -AuNP	HQ	1.539 $\mu\text{A } \mu\text{M}^{-1}$	4.3–150.0	1.28	4.25	100	DPV	2.0	This work
NDSBAC ¹	HQ	0.9997 μM	0.5–300	0.11	n.d.	112	DPV	6.5	[53]																																																																																																				
	CC	1.0662 μM	0.5–300	0.09	n.d.					WBC/Au-850-15 ²	HQ	164.4 $\mu\text{A } \mu\text{M}^{-1} \text{ cm}^{-2}$	0.008–1	0.002	n.d.	112.8	DPV	6.0	[54]	CC	132.0 $\mu\text{A } \mu\text{M}^{-1} \text{ cm}^{-2}$	0.01–1.0	0.004	n.d.	AuNPs-MPS ³	HQ	n.d.	10.0–1000.0	1.2	n.d.	123	SWV	7.0	[55]	CC	n.d.	30.0–1000.0	1.1	n.d.	GR-GO	HQ	n.d.	0.5–300	0.16	n.d.	102	DPV	7.0	[56]	CC	n.d.	0.5–300	0.2	n.d.	NiO/MWCNT	HQ	n.d.	10–500	2.5	n.d.	~110	DPV	7.0	[57]	CC	n.d.	10–400	2.5	n.d.	GO-TT-MWCNT	HQ	n.d.	0.01–200	0.035	n.d.	n.d.	DPV	7.4	[58]	CC	n.d.	0.5–200	0.049	n.d.	MWCNT-NH ₂ -AuNP	HQ	1.539 $\mu\text{A } \mu\text{M}^{-1}$	4.3–150.0	1.28	4.25	100	DPV	2.0	This work	CC	1.067 $\mu\text{A } \mu\text{M}^{-1}$	3.9–150.0	1.06	3.87										
WBC/Au-850-15 ²	HQ	164.4 $\mu\text{A } \mu\text{M}^{-1} \text{ cm}^{-2}$	0.008–1	0.002	n.d.	112.8	DPV	6.0	[54]																																																																																																				
	CC	132.0 $\mu\text{A } \mu\text{M}^{-1} \text{ cm}^{-2}$	0.01–1.0	0.004	n.d.					AuNPs-MPS ³	HQ	n.d.	10.0–1000.0	1.2	n.d.	123	SWV	7.0	[55]	CC	n.d.	30.0–1000.0	1.1	n.d.	GR-GO	HQ	n.d.	0.5–300	0.16	n.d.	102	DPV	7.0	[56]	CC	n.d.	0.5–300	0.2	n.d.	NiO/MWCNT	HQ	n.d.	10–500	2.5	n.d.	~110	DPV	7.0	[57]	CC	n.d.	10–400	2.5	n.d.	GO-TT-MWCNT	HQ	n.d.	0.01–200	0.035	n.d.	n.d.	DPV	7.4	[58]	CC	n.d.	0.5–200	0.049	n.d.	MWCNT-NH ₂ -AuNP	HQ	1.539 $\mu\text{A } \mu\text{M}^{-1}$	4.3–150.0	1.28	4.25	100	DPV	2.0	This work	CC	1.067 $\mu\text{A } \mu\text{M}^{-1}$	3.9–150.0	1.06	3.87																									
AuNPs-MPS ³	HQ	n.d.	10.0–1000.0	1.2	n.d.	123	SWV	7.0	[55]																																																																																																				
	CC	n.d.	30.0–1000.0	1.1	n.d.					GR-GO	HQ	n.d.	0.5–300	0.16	n.d.	102	DPV	7.0	[56]	CC	n.d.	0.5–300	0.2	n.d.	NiO/MWCNT	HQ	n.d.	10–500	2.5	n.d.	~110	DPV	7.0	[57]	CC	n.d.	10–400	2.5	n.d.	GO-TT-MWCNT	HQ	n.d.	0.01–200	0.035	n.d.	n.d.	DPV	7.4	[58]	CC	n.d.	0.5–200	0.049	n.d.	MWCNT-NH ₂ -AuNP	HQ	1.539 $\mu\text{A } \mu\text{M}^{-1}$	4.3–150.0	1.28	4.25	100	DPV	2.0	This work	CC	1.067 $\mu\text{A } \mu\text{M}^{-1}$	3.9–150.0	1.06	3.87																																								
GR-GO	HQ	n.d.	0.5–300	0.16	n.d.	102	DPV	7.0	[56]																																																																																																				
	CC	n.d.	0.5–300	0.2	n.d.					NiO/MWCNT	HQ	n.d.	10–500	2.5	n.d.	~110	DPV	7.0	[57]	CC	n.d.	10–400	2.5	n.d.	GO-TT-MWCNT	HQ	n.d.	0.01–200	0.035	n.d.	n.d.	DPV	7.4	[58]	CC	n.d.	0.5–200	0.049	n.d.	MWCNT-NH ₂ -AuNP	HQ	1.539 $\mu\text{A } \mu\text{M}^{-1}$	4.3–150.0	1.28	4.25	100	DPV	2.0	This work	CC	1.067 $\mu\text{A } \mu\text{M}^{-1}$	3.9–150.0	1.06	3.87																																																							
NiO/MWCNT	HQ	n.d.	10–500	2.5	n.d.	~110	DPV	7.0	[57]																																																																																																				
	CC	n.d.	10–400	2.5	n.d.					GO-TT-MWCNT	HQ	n.d.	0.01–200	0.035	n.d.	n.d.	DPV	7.4	[58]	CC	n.d.	0.5–200	0.049	n.d.	MWCNT-NH ₂ -AuNP	HQ	1.539 $\mu\text{A } \mu\text{M}^{-1}$	4.3–150.0	1.28	4.25	100	DPV	2.0	This work	CC	1.067 $\mu\text{A } \mu\text{M}^{-1}$	3.9–150.0	1.06	3.87																																																																						
GO-TT-MWCNT	HQ	n.d.	0.01–200	0.035	n.d.	n.d.	DPV	7.4	[58]																																																																																																				
	CC	n.d.	0.5–200	0.049	n.d.					MWCNT-NH ₂ -AuNP	HQ	1.539 $\mu\text{A } \mu\text{M}^{-1}$	4.3–150.0	1.28	4.25	100	DPV	2.0	This work	CC	1.067 $\mu\text{A } \mu\text{M}^{-1}$	3.9–150.0	1.06	3.87																																																																																					
MWCNT-NH ₂ -AuNP	HQ	1.539 $\mu\text{A } \mu\text{M}^{-1}$	4.3–150.0	1.28	4.25	100	DPV	2.0	This work																																																																																																				
	CC	1.067 $\mu\text{A } \mu\text{M}^{-1}$	3.9–150.0	1.06	3.87																																																																																																								

¹ Nitrogen-doped activated carbon derived from sugarcane bagasse. ² Gold nanoparticles decorated the seedling of white myoga ginger-derived biochar. ³ Gold nanoparticles mesoporous silica modified carbon paste electrode.

Comparing the results for the simultaneous determination of HQ and CT with electrodes modified with other materials reported in the literature (Table 2), the electrode modified with GCE/MWCNT-NH₂-AuNP achieves a higher sensitivity, good lineal range and a comparative ΔE_p in comparison with those obtained with electrodes modified with similar materials.

Considering the conducted studies and the electroanalytical response obtained with the GCE/MWCNT-NH₂-AuNP electrode, we worked on the simultaneous determination of these dihydroxybenzene isomers in a real matrix.

3.5. Reproducibility Study of the Modified Electrode Area with Nanostructured Material

Reproducibility assays were performed for GCE/MWCNT-NH₂ and GCE/MWCNT-NH₂-AuNP. In addition, the response of an unmodified GCE was studied as a control. For the study of reproducibility, ten electrodes ($n = 10$) were modified independently to analyze a concentration of 50.0 μM of HQ on the same day. Table S3 resumes the current values and the variation coefficients for the analyses. A variation coefficient of 3.12, 9.03 and 13.51% was obtained for GCE, GCE/MWCNT-NH₂ and GCE/MWCNT-NH₂-AuNP, respectively. This variability in the current measured could be attributed to the differences in the electroactive areas of the electrodes modified with the nanomaterials. MWCNTs are hydrophobic and, therefore, present difficulties to be scattered in water, even though the dispersions were sonicated in an ultrasound bath for one hour to minimize the agglomeration of the material. These agglomerates generate two effects: (i) different agglomerates sizes, which implies that not always will be the same amount of nanomaterial on the electrode surface, and (ii) reduced efficiency in current, due to the loss of nanomaterial behavior and prevails of the macrometric properties of carbon materials.

3.6. Determination of HQ and CT in Different Aqueous Matrices

HQ and CT were determinate in different aqueous matrices, which are from natural: drinking water, winery wastewater and river water. Standard addition analyses were

performed since this type of calibration strategy is used for the analytical determination in matrices that have a considerable matrix effect, and an external calibration is not allowed. A comparison of the standard addition results obtained in each matrix was conducted.

Table 2. Standard addition determination of hydroquinone ($n = 10$) in different aqueous matrices by differential pulse voltammetry, recovery coefficients and experimental t ($\alpha = 0.05$) for each determination made.

Matrix	Analyte	Concentration (μM)	Obtained Concentration (μM)	Recovery (%)
Drinking water	HQ	55.0	48.6 ± 0.7	88.4
	CT		45.3 ± 0.5	82.4
Viticultural wastewater	HQ	145.0	75.8 ± 0.8	52.3
	CT		71.5 ± 0.4	49.3
River water	HQ	100.0	80.3 ± 0.5	80.3
	CT		84.2 ± 0.6	84.2

In this case, DPV was employed for the analysis of aggregated hydroquinone using the methodology developed in this work. The method developed was applied to the determination of hydroquinone in different aqueous matrices, which are both of natural origin and water treated for consumption. The determination of hydroquinone and catechol were performed by differential pulse voltammetry, obtaining the results shown in Table 2. The linear range of the analyte in the matrices studied was smaller than the working range obtained using standard MilliQ water. In addition, a reduced slope can be observed when determining the analyte in all the matrices. Recovery values under 88.4% were obtained in all the studied matrices, except for winery water, which has a very low recovery rate (less than 53.0%). The low recovery for fortified winery wastewater can be attributed to the effect of the matrix on determination, and there may be species that are consuming the hydroquinone added in the sample. In addition to this, all the matrices present a high amount of unidentified interferents, such as inorganic ions, chlorides, polyphenols and organic species that could interfere with the electrochemical oxidation of the dihydroxy-benzenes studied in this work. In this way, analyzing hydroquinone and its isomers would be possible, as well as molecules that have dihydroxy-benzenes groups present in their structure, with low accuracy.

Considering the obtained results, it was proposed to use the wine wastewater for the application of a multivariate strategy for the quantification of hydroquinone and catechol since this matrix is the one that presents the lowest recovery levels, and the matrix has a greater quantity of interferents that hinder the determination of analytes.

3.7. Evaluation of Multivariate Calibration Method for Simultaneous Determination of HQ and CT

A model based on PLS was built for the determination of HQ and CT in industrial residues of the wine industry. Best results were obtained by applying a baseline correction and \log_{10} to compensate the dispersion of the baseline current between each measurement made due to the reproducibility of the electrodes. Voltammograms were preprocessed, and a mean center was applied to avoid variation of the oxidation potential of HQ and CT between the measurements for the fortified samples. Two latent variables were selected for the HQ model and 3 latent variables for the CT model. This number of variables exhibits the lowest validation errors by cross-validation, allowing a more accurate determination because this number of components delivers a lower residual error. In addition, the analytical figures of merit were obtained for each model based on the PLS model obtained. These results are presented in Table S4. From the information obtained from the multivariate model, HQ and CT can be determined simultaneously in a range of 1.0–126.0 μM for

HQ and from 7.0–177.0 μM for CT, with calibration and validation errors close to 20% obtained by cross-validation. The PLS model was evaluated using an 8-sample validation set for wine industry wastewaters, fortified with known analyte concentrations. Standard prediction errors (SEP) of 9.9% were obtained for HQ quantification and 8.4% for CT in simultaneous quantification of both analytes in the wastewater. The charts with the values of SEP and the HQ and CT real concentrations versus predicted concentrations of both analytes are presented in Figure 6. This figure shows graphically the correlation between the known analyte concentrations (Y observed) and the concentrations predicted by the model (Y predicted), where the line represents the predicted ideal values when evaluating the voltammogram obtained by DPV in the vector of regression B, where greater proximity of the points to the line indicates a good accuracy in the prediction of the concentration. According to the results obtained, the values predicted by the PLS model are concordant with the concentrations added to the real sample, having a low prediction error.

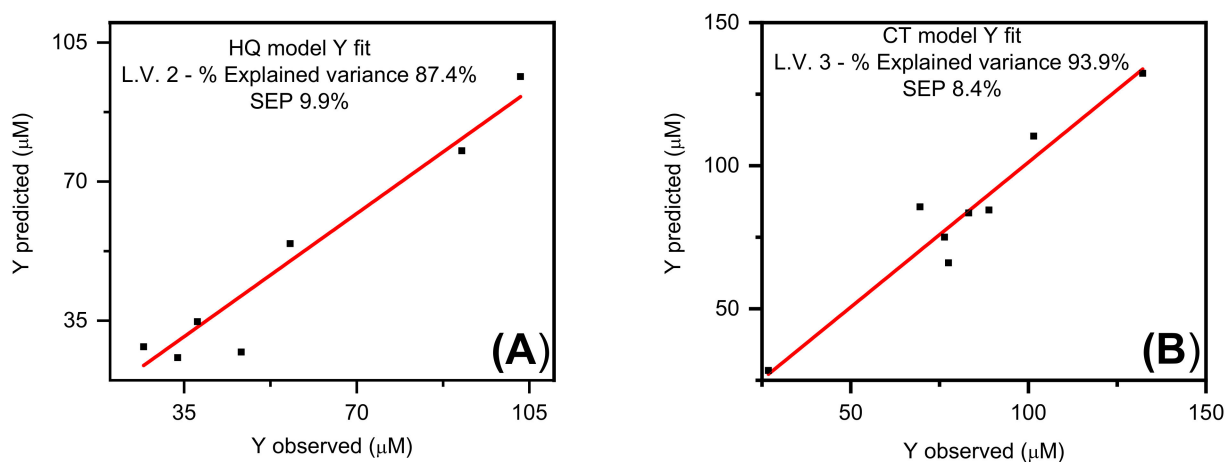


Figure 6. Plot of (A) HQ and (B) CT predicted concentrations as a function of the nominal values in validation samples for determination in wine industry wastewater by PLS calibration model.

Finally, the built model has high SEC and SEV values. This indicates preliminary that the model is not very robust for the simultaneous determination of HQ and CT. Nevertheless, a good correlation is observed between the values predicted by the models and concentrations used in sample fortifications when compared with standard addition in studies with real samples. To compare simultaneously the predictive capability of the studied methods, the predicted values obtained in this work are shown in Figure 7. Elliptical Joint Confidence Region (EJCR) is employed to analyze the performance of standard addition and PLS quantification in terms of normalized values of 1 for slope and 0 for the intercept of each calibration methodology presented in this work and can include their confidence ranges around the means. The amplitude of the ellipse acts as a precision indicator, where a wide ellipse implies larger confidence intervals and a lower precision, and a small ellipse indicates a higher precision for that calibration method. Additionally, if the ellipse contains the normalized value (point located at $\{x,y\} = 1,0$), it indicates graphically how accurate is the calibration method used.

Figure 7 shows that the low accuracy and precision of standard addition makes it not suitable for the real samples. Instead, standard addition to analytical-grade water combined with the PLS model yield more accurate predictions. The effect on bias is present in the ellipse obtained for the simultaneous quantification of HQ and CT in standard addition applied to real samples. Therefore, it can be inferred that there is an error produced by the matrix effect exerted by electroactive species that can interfere with the electrochemical determination or by species present in the sample that can inactivate the electrode. This error would prevent the electronic transfer from the analyte to the electrode and generate interference in the electrochemical signal from the redox process of HQ and CT.

Regarding the precision of the methods, both the standard addition to MilliQ water and the determination via PLS are more accurate and precise than the simultaneous analysis of both dihydroxy-benzene isomers using standard addition in real samples. According to the results obtained, a multivariate methodology would be more suitable for the analysis of real samples, as they reduce the matrix effect on the determination of both analytes simultaneously and result in accurate and precise electrochemical determinations.

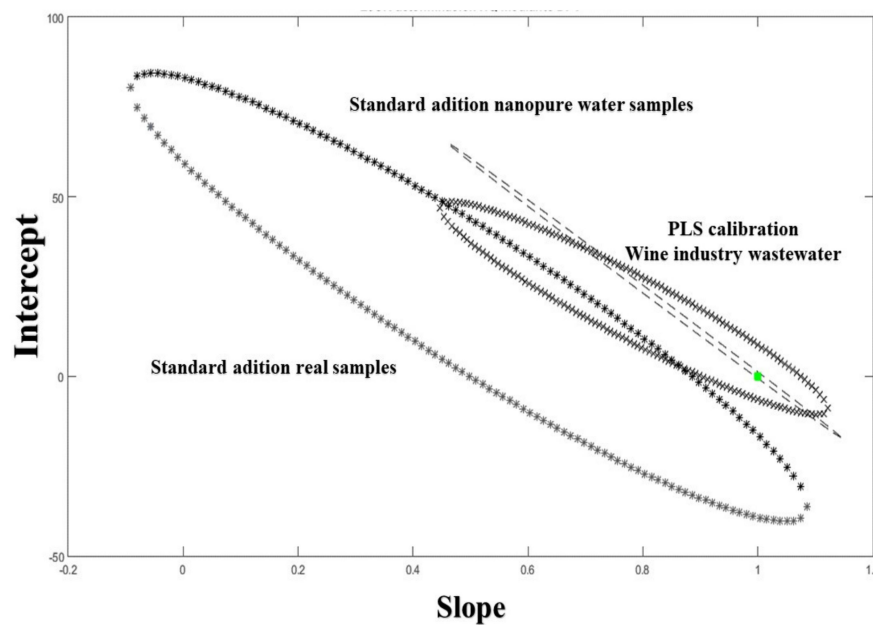


Figure 7. Elliptical joint region (at 95% confidence level) for the slope and intercept of predicted vs. nominal concentrations predicted by standard addition and the PLS model developed in this work. The green cross marks the theoretical (intercept = 0, slope = 1) point.

The results obtained in this work indicate that chemometric multivariate calibration tools, such as PLS, are adequate and better than classical calibration methods used in electrochemistry like standard addition for the direct and electrochemical simultaneous determination of HQ and CT in real samples, even in the absence of interference considered in the development of the methodology, which achieved errors lower than 10% in the quantification of the analytes.

4. Conclusions

The electrochemical oxidation of HQ in aqueous media showed a higher current response and lower ΔE_p when using electrodes modified with multiple-walled carbon nanotubes (MWCNT), oxidized multiple-walled carbon nanotubes (MWCNT-COOH) and amino carbon nanotubes (MWCNT-NH₂), compared to the unmodified carbon electrode. The redox response of HQ presented a signal of higher current intensity when using electrodes modified with oxidized multiple-walled carbon nanotubes (MWCNT-COOH) and amine multiple-walled carbon nanotubes (MWCNT-NH₂); however, the latter presented a more defined signal. The redox response of HQ increased by simultaneously modifying the electrodes with MWCNT-NH₂ and gold nanospheres (AuNP), further allowing separation with their structural isomers in the same solution.

An electroanalytical methodology was developed that allows the determination of HQ and CT in nanopure water, with a LOD of 1.0 μM in a working range of 4.0 to 150.0 μM and an approximated error of 2.0%.

In real samples, the simultaneous determination of HQ and CT presented recoveries of less than 88.4% in drinking water and winery wastewater. A multivariate model was

constructed by PLS, achieving prediction errors at 9.9% for HQ and 8.4% for CT with minimal sample treatment.

Supplementary Materials: The following are available online at <https://www.mdpi.com/article/10.3390/chemosensors9050088/s1>, Table S1: Current and potential values for the oxidation and reduction of HQ using the different systems of CNT, Table S2: HQ oxidation peak potentials and currents obtained using the different AuNS and CNT systems, Table S3: Current values obtained for independently modified electrodes (n = 10) for the oxidation of 50.0 μ M hydroquinone by differential pulse voltammetry, Table S4: Analytical figures of merit of the PLS models constructed for the simultaneous determination of HQ and CT, Figure S1: Effect of pH on oxidation current intensity of 0.1 mM HQ for GCE/MWCNT-NH₂ and GCE/MWCNT-COOH systems, Figure S2: Size distribution of AuNS obtained using DLS.

Author Contributions: S.P., C.C.-O., P.J.-U. and R.S. conceived, designed the experiments, discussed the results and made a first draft of the paper. S.P., C.C.-O., P.J.-U. and N.H. performed the experiments and the data treatment. D.C. revised the writing of the paper from the first draft to the definitive version. All authors have read and agreed to the published version of the manuscript.

Funding: This research was funded by FONDECYT Grant 1170352, DICYT-USACH project 0221425G_P OSTDOC, and CONICYT/ANID PhD fellowships N° 21,160,955 & N° 21,190,322 awarded to C. Candia-Onfray and S. Piña Hodges, respectively.

Institutional Review Board Statement: Not applicable.

Informed Consent Statement: Not applicable.

Data Availability Statement: Data available in a publicly accessible repository.

Acknowledgments: We are grateful to FONDECYT Grant 1170352, DICYT-USACH and CONICYT/ANID PhD fellowship N° 21,160,955 & N° 21,190,322 awarded to C. Candia-Onfray and S. Piña Hodges, respectively.

Conflicts of Interest: The authors declare no conflict of interest.

References

1. Zhang, Y.; Bin Zheng, J. Comparative investigation on electrochemical behavior of hydroquinone at carbon ionic liquid electrode, ionic liquid modified carbon paste electrode and carbon paste electrode. *Electrochim. Acta* **2007**, *52*, 7210–7216. [[CrossRef](#)]
2. Vilela, C.L.S.; Bassin, J.P.; Peixoto, R.S. Water contamination by endocrine disruptors: Impacts, microbiological aspects and trends for environmental protection. *Environ. Pollut.* **2018**, *235*, 546–559. [[CrossRef](#)]
3. Liu, W.; Tao, F.; Zhang, W.; Li, S.; Zheng, M. Contamination and emission factors of PCDD/Fs, unintentional PCBs, HxCBz, PeCBz and polychlorophenols in chloranil in China. *Chemosphere* **2012**, *86*, 248–251. [[CrossRef](#)] [[PubMed](#)]
4. Gmurek, M.; Olak-Kucharczyk, M.; Ledakowicz, S. Photochemical decomposition of endocrine disrupting compounds—A review. *Chem. Eng. J.* **2017**, *310*, 437–456. [[CrossRef](#)]
5. Omar, T.F.T.; Ahmad, A.; Aris, A.Z.; Yusoff, F.M. Endocrine Disrupting Compounds (EDCs) in environmental matrices: Review of analytical strategies for pharmaceuticals, estrogenic hormones, and alkylphenol compounds. *TrAC Trends Anal. Chem.* **2016**, *85*, 241–259. [[CrossRef](#)]
6. Aragón, M.; Ariño, C.; Dago, À.; Díaz-Cruz, J.M.; Esteban, M. Simultaneous determination of hydroquinone, catechol and resorcinol by voltammetry using graphene screen-printed electrodes and partial least squares calibration. *Talanta* **2016**, *160*, 138–143. [[CrossRef](#)]
7. Lawal, A.T. Progress in utilisation of graphene for electrochemical biosensors. *Biosens. Bioelectron.* **2018**, *106*, 149–178. [[CrossRef](#)]
8. Qin, L.; Zeng, G.; Lai, C.; Huang, D.; Xu, P.; Zhang, C.; Cheng, M.; Liu, X.; Liu, S.; Li, B.; et al. “Gold rush” in modern science: Fabrication strategies and typical advanced applications of gold nanoparticles in sensing. *Coord. Chem. Rev.* **2018**, *359*, 1–31. [[CrossRef](#)]
9. Gupta, S.; Murthy, C.; Prabha, C.R. Recent advances in carbon nanotube based electrochemical biosensors. *Int. J. Biol. Macromol.* **2018**, *108*, 687–703. [[CrossRef](#)]
10. Rashidiani, J.; Kamali, M.; Sedighian, H.; Akbariomi, M.; Mansouri, M.; Kooshki, H. Ultrahigh sensitive enhanced-electrochemiluminescence detection of cancer biomarkers using silica NPs/graphene oxide: A comparative study. *Biosens. Bioelectron.* **2018**, *102*, 226–233. [[CrossRef](#)]
11. Govindasamy, M.; Manavalan, S.; Chen, S.-M.; Rajaji, U.; Chen, T.-W.; Al-Hemaid, F.M.A.; Ali, M.A.; Elshikh, M.S. Determination of neurotransmitter in biological and drug samples using gold nanorods decorated-MWCNTs modified electrode. *J. Electrochem. Soc.* **2018**, *165*, B370–B377. [[CrossRef](#)]

12. Peng, C.; Li, Z.; Zhang, X.; Zhou, S.; Zhang, W.; Liu, X.; Zhao, P. Simultaneous determination of hydroquinone, catechol and resorcinol with high selectivity based on hollow nitrogen-doped mesoporous carbon spheres decorated graphene. *J. Electrochem. Soc.* **2018**, *165*, B212–B219. [[CrossRef](#)]
13. Li, Y.; Li, Z.; Liu, H.; Chen, S.; Guo, X.; Lin, M.; Li, F. A portable electrochemical platform integrated with a 3D AuNPs/CNTs sponge for point-of-care testing of neurotransmitters. *J. Electrochem. Soc.* **2019**, *166*, B524–B531. [[CrossRef](#)]
14. Wang, J. Carbon-nanotube based electrochemical biosensors: A review. *Electroanalysis* **2005**, *17*, 7–14. [[CrossRef](#)]
15. Sedghi, R.; Pezeshkian, Z. Fabrication of non-enzymatic glucose sensor based on nanocomposite of MWCNTs-COOH-Poly(2-aminothiophenol)-Au NPs. *Sens. Actuators B Chem.* **2015**, *219*, 119–124. [[CrossRef](#)]
16. Żelechowska, K.; Trawiński, B.; Dramińska, S.; Majdecka, D.; Bilewicz, R.; Kusz, B. Oxygen biosensor based on carbon nanotubes directly grown on graphitic substrate. *Sens. Actuators B Chem.* **2017**, *240*, 1308–1313. [[CrossRef](#)]
17. Wong, A.; Foguel, M.V.; Khan, S.; de Oliveira, F.M.; Tarley, C.R.T.; Sotomayor, M.D. Development of an electrochemical sensor modified with MWCNT-COOH and MIP for detection of diuron. *Electrochim. Acta* **2015**, *182*, 122–130. [[CrossRef](#)]
18. Bu, C.; Liu, X.; Zhang, Y.; Li, L.; Zhou, X.; Lu, X. A sensor based on the carbon nanotubes-ionic liquid composite for simultaneous determination of hydroquinone and catechol. *Colloids Surf. B Biointerfaces* **2011**, *88*, 292–296. [[CrossRef](#)] [[PubMed](#)]
19. Ghoreishi, S.M.; Behpour, M.; Hajisadeghian, E.; Golestaneh, M. Voltammetric determination of resorcinol on the surface of a glassy carbon electrode modified with multi-walled carbon nanotube. *Arab. J. Chem.* **2016**, *9*, S1563–S1568. [[CrossRef](#)]
20. Nugent, J.M.; Santhanam, K.S.V.; Rubio, A.; Ajayan, P.M. Fast electron transfer kinetics on multiwalled carbon nanotube microbundle electrodes. *Nano Lett.* **2001**, *1*, 87–91. [[CrossRef](#)]
21. Liu, X.; Ding, Z.; He, Y.; Xue, Z.; Zhao, X.; Lu, X. Electrochemical behavior of hydroquinone at multi-walled carbon nanotubes and ionic liquid composite film modified electrode. *Colloids Surf. B Biointerfaces* **2010**, *79*, 27–32. [[CrossRef](#)]
22. Mendes, R.G.; Wróbel, P.S.; Bachmatiuk, A.; Sun, J.; Gemming, T.; Liu, Z.; Rummeli, M.H. Carbon nanostructures as a multi-functional platform for sensing applications. *Chemosensors* **2018**, *6*, 60. [[CrossRef](#)]
23. Campbell, F.W.; Compton, R.G. The use of nanoparticles in electroanalysis: An updated review. *Anal. Bioanal. Chem.* **2009**, *396*, 241–259. [[CrossRef](#)]
24. Katz, E.; Willner, I.; Wang, J. Electroanalytical and bioelectroanalytical systems based on metal and semiconductor nanoparticles. *Electroanalysis* **2004**, *16*, 19–44. [[CrossRef](#)]
25. Sebarchievici, I.; Taranu, B.O.; Birdeanu, M.; Rus, S.F.; Fagadar-Cosma, E. Electrocatalytic behaviour and application of manganese porphyrin/gold nanoparticle- surface modified glassy carbon electrodes. *Appl. Surf. Sci.* **2016**, *390*, 131–140. [[CrossRef](#)]
26. Turkevich, J.; Stevenson, P.C.; Hillier, J. A study of the nucleation and growth processes in the synthesis of colloidal gold. *Discuss. Faraday Soc.* **1951**, *11*, 55–75. [[CrossRef](#)]
27. Xia, H.; Bai, S.; Hartmann, J.; Wang, D. Synthesis of monodisperse quasi-spherical gold nanoparticles in water via silver(I)-assisted citrate reduction. *Langmuir* **2010**, *26*, 3585–3589. [[CrossRef](#)] [[PubMed](#)]
28. Jin, W.; Maduraiveeran, G. Electrochemical detection of chemical pollutants based on gold nanomaterials. *Trends Environ. Anal. Chem.* **2017**, *14*, 28–36. [[CrossRef](#)]
29. Petrović, S.; Guzsány, V.; Ranković, N.; Beljin, J.; Rončević, S.; Dalmacija, B.; Ashrafi, A.M.; Kónya, Z.; Švancara, I.; Vytřas, K. Trace level voltammetric determination of Zn(II) in selected nutrition related samples by bismuth-oxochloride-multiwalled carbon nanotube composite based electrode. *Microchem. J.* **2019**, *146*, 178–186. [[CrossRef](#)]
30. Bounegru, A.V.; Apetrei, C. Voltammetric sensors based on nanomaterials for detection of caffeic acid in food supplements. *Chemosensors* **2020**, *8*, 41. [[CrossRef](#)]
31. Cui, H.; He, C.X.; Zhao, G.W. Determination of polyphenols by HPLC with inhibited chemiluminescence detection. *J. Chromatogr. A* **1999**, *855*, 171–179. [[CrossRef](#)]
32. Moldoveanu, S.C.; Kiser, M. Gas chromatography/mass spectrometry versus liquid chromatography/fluorescence detection in the analysis of phenols in mainstream cigarette smoke. *J. Chromatogr. A* **2007**, *1141*, 90–97. [[CrossRef](#)]
33. Elghobashy, M.R.; Bebawy, L.I.; Shokry, R.F.; Abbas, S.S. Successive ratio subtraction coupled with constant multiplication spectrophotometric method for determination of hydroquinone in complex mixture with its degradation products, tretinoin and methyl paraben. *Spectrochim. Acta Part A Mol. Biomol. Spectrosc.* **2016**, *157*, 116–123. [[CrossRef](#)]
34. Patil, S.K.; Patil, S.A.; Vadiyar, M.M.; Awale, D.V.; Sartape, A.S.; Walekar, L.S.; Kolekar, G.B.; Ghorpade, U.V.; Kim, J.H.; Kolekar, S.S. Tailor-made dicationic ionic liquid as a fluorescent sensor for detection of hydroquinone and catechol. *J. Mol. Liq.* **2017**, *244*, 39–45. [[CrossRef](#)]
35. Karim-Nezhad, G.; Moghaddam, M.H.; Khorablou, Z.; Dorraji, P.S. L-cysteine based polymer matrix decorated with au-nanoparticles: As a sensing platform for simultaneous determination of hydroquinone and catechol. *J. Electrochem. Soc.* **2017**, *164*, B193–B199. [[CrossRef](#)]
36. Ahammad, A.J.S.; Akter, T.; Mamun, A.; Islam, T.; Hasan, M.; Mamun, M.A.; Faraezi, S.; Monira, F.Z.; Saha, J.K. Cost-effective electrochemical sensor based on carbon nanotube modified-pencil electrode for the simultaneous determination of hydroquinone and catechol. *J. Electrochem. Soc.* **2018**, *165*, B390–B397. [[CrossRef](#)]
37. Otto, M. *Chemometrics: Statics and Computer Application in Analytical Chemistry*, 3rd ed.; Wiley: Weinheim, Germany, 2017; ISBN 9783527340972.
38. Kumar, N.; Bansal, A.; Sarma, G.; Rawal, R.K. Chemometrics tools used in analytical chemistry: An overview. *Talanta* **2014**, *123*, 186–199. [[CrossRef](#)] [[PubMed](#)]

39. Xu, G.; Li, B.; Luo, X. Carbon nanotube doped poly(3,4-ethylenedioxythiophene) for the electrocatalytic oxidation and detection of hydroquinone. *Sens. Actuators B Chem.* **2013**, *176*, 69–74. [[CrossRef](#)]
40. Liu, Y.; Liao, H.; Zhou, Y.; Du, Y.; Wei, C.; Zhao, J.; Sun, S.; Loo, J.S.; Xu, Z.J. Fe₂O₃ nanoparticle/SWCNT composite electrode for sensitive electrocatalytic oxidation of hydroquinone. *Electrochim. Acta* **2015**, *180*, 1059–1067. [[CrossRef](#)]
41. Zhang, X.P.; Jiang, W.L.; Cao, S.H.; Sun, H.J.; You, X.Q.; Cai, S.H.; Wang, J.L.; Zhao, C.S.; Wang, X.; Chen, Z.; et al. NMR spectroelectrochemistry in studies of hydroquinone oxidation by polyaniline thin films. *Electrochim. Acta* **2018**, *273*, 300–306. [[CrossRef](#)]
42. Naqvi, S.T.R.; Rasheed, T.; Hussain, D.; Haq, M.N.U.; Majeed, S.; Shafi, S.; Ahmed, N.; Nawaz, R. Modification strategies for improving the solubility/dispersion of carbon nanotubes. *J. Mol. Liq.* **2020**, *297*, 111919. [[CrossRef](#)]
43. Hu, Y.; Li, D.; Tang, P.; Bin, Y.; Wang, H. Comparative study of structure, mechanical and electromagnetic interference shielding properties of carbon nanotube buckypapers prepared by different dispersion media. *Mater. Des.* **2019**, *184*, 108175. [[CrossRef](#)]
44. Cañete-Rosales, P.; Ortega, V.; Álvarez-Lueje, A.; Bollo, S.; González, M.; Anson, A.; Martínez, M.T. Influence of size and oxidative treatments of multi-walled carbon nanotubes on their electrocatalytic properties. *Electrochim. Acta* **2012**, *62*, 163–171. [[CrossRef](#)]
45. Ganesh, P.; Swamy, B.K. Simultaneous electroanalysis of hydroquinone and catechol at poly(brilliant blue) modified carbon paste electrode: A voltammetric study. *J. Electroanal. Chem.* **2015**, *756*, 193–200. [[CrossRef](#)]
46. Tserpes, K.; Silvestre, N. *Modeling of Carbon Nanotubes, Graphene and Their Composites*; Springer International Publishing: Berlin/Heidelberg, Germany, 2014; ISBN 9783319012001.
47. Zhang, Y.; Kang, Z. Highly conductive and anticorrosion Ag/CNTs/NDs hybrid films on molecular-grafted PET substrate for flexible electrodes. *Appl. Surf. Sci.* **2018**, *427*, 282–292. [[CrossRef](#)]
48. Richard, G.C.; Batchelor-McAuley, C.; Dickinson, E.J.F. *Understanding Voltammetry: Problems and Solutions*; Imperial College Press: London, UK, 2012; ISBN 9781848167308.
49. Yang, C.; Denno, M.E.; Pyakurel, P.; Venton, B.J. Recent trends in carbon nanomaterial-based electrochemical sensors for biomolecules: A review. *Anal. Chim. Acta* **2015**, *887*, 17–37. [[CrossRef](#)]
50. Alim, S.; Vejjayan, J.; Yusoff, M.M.; Kafi, A. Recent uses of carbon nanotubes & gold nanoparticles in electrochemistry with application in biosensing: A review. *Biosens. Bioelectron.* **2018**, *121*, 125–136. [[CrossRef](#)] [[PubMed](#)]
51. Olivieri, A.C. Practical guidelines for reporting results in single- and multi-component analytical calibration: A tutorial. *Anal. Chim. Acta* **2015**, *868*, 10–22. [[CrossRef](#)] [[PubMed](#)]
52. Miller, J.N. Basic statistical methods for analytical chemistry. Part 2. Calibration and regression methods. A review. *Analyst* **1991**, *116*, 3–14. [[CrossRef](#)]
53. Zheng, X.; Fan, R.; Hu, Y.; Zhong, H.; Yang, X.; Lv, R.; Yang, X.; Huang, B. Selective and simultaneous determination of hydroquinone and catechol by using a nitrogen-doped bagasse activated carbon modified electrode. *Mater. Chem. Phys.* **2020**, *242*, 122525. [[CrossRef](#)]
54. Wang, J.; Yang, J.; Xu, P.; Liu, H.; Zhang, L.; Zhang, S.; Tian, L. Gold nanoparticles decorated biochar modified electrode for the high-performance simultaneous determination of hydroquinone and catechol. *Sens. Actuators B Chem.* **2020**, *306*, 127590. [[CrossRef](#)]
55. Tashkhourian, J.; Daneshi, M.; Nami-Ana, F.; Behbahani, M.; Bagheri, A. Simultaneous determination of hydroquinone and catechol at gold nanoparticles mesoporous silica modified carbon paste electrode. *J. Hazard. Mater.* **2016**, *318*, 117–124. [[CrossRef](#)] [[PubMed](#)]
56. Zhou, X.; He, Z.; Lian, Q.; Li, Z.; Jiang, H.; Lu, X. Simultaneous determination of dihydroxybenzene isomers based on graphene-graphene oxide nanocomposite modified glassy carbon electrode. *Sens. Actuators B Chem.* **2014**, *193*, 198–204. [[CrossRef](#)]
57. Zhao, L.; Yu, J.; Yue, S.; Zhang, L.; Wang, Z.; Guo, P.; Liu, Q. Nickel oxide/carbon nanotube nanocomposites prepared by atomic layer deposition for electrochemical sensing of hydroquinone and catechol. *J. Electroanal. Chem.* **2018**, *808*, 245–251. [[CrossRef](#)]
58. Han, H.S.; You, J.-M.; Seol, H.; Jeong, H.; Jeon, S. Electrochemical sensor for hydroquinone and catechol based on electrochemically reduced GO-terthiophene-CNT. *Sens. Actuators B Chem.* **2014**, *194*, 460–469. [[CrossRef](#)]